Axoplasmic Reticulum Ca^{2+} Release Causes Secondary Degeneration of Spinal Axons

David P. Stirling, PhD,[1,2] Karen Cummins,[1]
S. R. Wayne Chen, PhD,[3] and Peter Stys, MD[1]

Objective: Transected axons of the central nervous system fail to regenerate and instead die back away from the lesion site, resulting in permanent disability. Although both intrinsic (eg, microtubule instability, calpain activation) and extrinsic (ie, macrophages) processes are implicated in axonal dieback, the underlying mechanisms remain uncertain. Furthermore, the precise mechanisms that cause delayed "bystander" loss of spinal axons, that is, ones that were not directly damaged by the initial insult, but succumbed to secondary degeneration, remain unclear. Our goal was to evaluate the role of intra-axonal Ca^{2+} stores in secondary axonal degeneration following spinal cord injury.
Methods: We developed a 2-photon laser-induced spinal cord injury model to follow morphological and Ca^{2+} changes in live myelinated spinal axons acutely following injury.
Results: Transected axons "died back" within swollen myelin or underwent synchronous pan-fragmentation associated with robust Ca^{2+} increases. Spared fibers underwent delayed secondary bystander degeneration. Reducing Ca^{2+} release from axonal stores mediated by ryanodine and inositol triphosphate receptors significantly decreased axonal dieback and bystander injury. Conversely, a gain-of-function ryanodine receptor 2 mutant or pharmacological treatments that promote axonal store Ca^{2+} release worsened these events.
Interpretation: Ca^{2+} release from intra-axonal Ca^{2+} stores, distributed along the length of the axon, contributes significantly to secondary degeneration of axons. This refocuses our approach to protecting spinal white matter tracts, where emphasis has been placed on limiting Ca^{2+} entry from the extracellular space across cell membranes, and emphasizes that modulation of axonal Ca^{2+} stores may be a key pharmacotherapeutic goal in spinal cord injury.

ANN NEUROL 2014;75:220–229

Injured axons of the central nervous system (CNS) and peripheral nervous system undergo degeneration of segments distal to the injury site by a process termed Wallerian degeneration.[1] Unlike peripheral axons that regenerate from their proximal stumps after injury, transected axons of the CNS fail to regrow and instead die back away from the lesion site. Although both intrinsic (eg, microtubule instability, calpain activation)[2,3] and extrinsic (ie, macrophages)[4–6] processes have been implicated in axonal dieback, the underlying mechanisms of this potentially critical phenomenon contributing to failure of repair remain poorly understood. Understanding and overcoming this failure of CNS axonal regeneration is a key objective in the field of spinal cord injury (SCI).[7] Furthermore, the precise mechanisms that cause delayed "bystander" loss of spinal axons, that is, ones that were not directly damaged by the initial insult, but succumbed to secondary degeneration, remain unclear. Based on our previous work on the role of intra-axonal Ca^{2+} stores release in white matter injury,[8] we hypothesized that a similar mechanism might play an important role both in local (ie, near the injury site) and remote (ie, at a considerable distance from the injury) degeneration of axons following a focal insult. Given the unusual

View this article online at wileyonlinelibrary.com. DOI: 10.1002/ana.24099

Received May 14, 2013, and in revised form Nov 29, 2013. Accepted for publication Dec 26, 2013.

Address correspondence to Dr Stys, HRIC Bldg, RM 1AA22, 3330 Hospital Drive NW, Calgary, Alberta, Canada T2N 4N1.
E-mail address: pstys@ucalgary.ca and Dr Stirling MDR Bldg, RM 608, 511 S. Floyd Street Louisville, Kentucky, USA 40292. E-mail address: david.stirling@louisville.edu

From the [1]Department of Clinical Neurosciences, Hotchkiss Brain Institute, University of Calgary, Calgary, Alberta, Canada; [2]Kentucky Spinal Cord Injury Research Center and Departments of Neurological Surgery, Microbiology and Immunology, University of Louisville, Louisville, KY; [3]Department of Physiology and Pharmacology, Libin Cardiovascular Institute of Alberta, University of Calgary, Calgary, Alberta, Canada.

Additional Supporting Information may be found in the online version of this article.

geometry of axons, whose length can extend enormous distances relative to the size of the parent soma, and the endomembrane system composed of axoplasmic reticulum thought to extend over long distances within the fiber,[9,10] a self-propagating wave of deleterious intra-axonal Ca^{2+} triggered by a localized injury may spatially extend axonal damage and thus make successful regeneration an even more difficult goal.

Materials and Methods

Mice

Experiments were approved by the University of Calgary Animal Care Ethics Committee as outlined in the guidelines of the Canadian Council on Animal Care. Thy1-yellow fluorescent protein $(YFP)^+$ mice (Jackson Laboratory, Bar Harbor, ME) were used to visualize dorsal column axons. Ryanodine receptor 2 (RyR2) homozygous gain-of-function knock-in mice (RyR2 R4496C$^{+/+}$) and littermate controls (RyR2 R4496C$^{-/-}$)[36], or C57BL/6 mice (Charles River Laboratories, Senneville, Quebec, Canada) were used for bath loading of Ca^{2+} indicators and tracers.

Ex Vivo Live Whole Spinal Cord Model

Following anesthesia, mice were perfused with ice cold, oxygenated low Ca^{2+} artificial cerebrospinal fluid (aCSF; in mM: NaCl 126, $NaHCO_3$ 26, KCl 3, NaH_2PO_4 1.25, $MgSO_4$ 2, $CaCl_2$ 0.1, and dextrose 10), and spinal cords were removed and placed in a customized imaging chamber (RC-27L Large Bath Chamber; Harvard Apparatus Canada, Saint-Laurent, Quebec, Canada). The perfusate was then slowly changed to oxygenated 2mM Ca^{2+} aCSF, maintained at 36.5°C via an in-line heater (Harvard Apparatus Canada) and an objective heater system (Bioptechs, Butler, PA). To visualize myelin, the lipophilic dye Nile Red (catalog number N-1142; Life Technologies, Burlington, Ontario, Canada) was first dissolved in dimethylsulfoxide and used at a final concentration of 25 μM, then directly and briefly added to the perfusion chamber in 2μl volumes until clear labeling of myelin surrounding YFP^+ axon profiles was obtained.

Microscopy

Time-lapse 2-photon–excited images were collected using a custom modified microscope (Nikon D-Eclipse C1; Nikon Instruments, Tokyo, Japan). Briefly, fluorescent proteins and dyes were excited using 950nm, 10- to 15mW laser pulses from a Ti:sapphire laser (Tsunami; Spectra-Physics, Santa Clara, CA), filtered through 525 ± 25nm and 590nm long-pass filters (Chroma Technology, Bellows Falls, VT), and detected with a pair of photomultiplier tubes (R5929; Hamamatsu Photonics, Hamamatsu, Japan).

Laser-induced SCI

To ablate dorsal column fibers, the area over the gracile fasciculus was magnified ×11.9 (17.81 × 17.81 μm, area = 317.20 μm^2), the laser tuned to 800nm, and power increased to 600mW into the scan head (≈50–75 mW at the sample) for 10 passes (1.92 microseconds pixel dwell time) to produce a highly reproducible axonal ablation by microplasma generation, and not by heat.[11,12] At the midcervical level of the spinal cord used for imaging, the axons of the gracile fasciculus are located close to midline and ascend from T6 and below, allowing differentiation between proximal (caudal) axonal dieback and distal (rostral) axonal degeneration, as we have done previously in vivo.[5,6]

Dye Loading of Live Ex Vivo Spinal Cords

To detect Ca^{2+} changes in axons, Thy1-YFP^+ or C57Bl/6 mouse spinal cords were incubated in low Ca^{2+} aCSF with the cell permeant Ca^{2+} indicator X-rhod-1 AM (20 μM, Life Technologies) or the Ca^{2+} indicator Oregon Green BAPTA-1 dextran (10,000 MW; 250 μM, Life Technologies) and Alexa 594 dextran (250 μM, Life Technologies) to outline axon profiles, as previously described.[13] To visualize axons, RyR2 R4496C$^{+/+}$ and wild-type littermate control spinal cords were incubated with Alexa Fluor 488 dextran (10,000 MW; 250 μM, catalog number D-22910, Life Technologies). Nile Red was added to the perfusion chamber to label myelin only in noncalcium imaging studies due to the overlap of the emission spectra of Nile Red and X-rhod-1.

Pharmacological Agents

Ryanodine (50 μM), 2-aminoethoxydiphenylborane (2-APB, 100 μM), thapsigargin (1 μM), and caffeine (0.5 mM), were purchased from Tocris Bioscience (Minneapolis, MN), and used as per the manufacturer's recommendations. All agents were added 30 minutes before laser-induced SCI (LiSCI) and continuously perfused for the duration of each experiment.

Image Analysis

Four-dimensional data were imported into ImageTrak (written by P.S.; http://www.ucalgary.ca/styslab/imagetrak). For axonal dieback distance quantification, a total of n = 24 to 141 axonal end bulbs per group, from 3 to 14 animals per group, were analyzed and expressed as median and 25th and 75th percentile (box and whisker plots), as the data were not normally distributed. Ablation width and area were measured using 5 individual adjacent images centered over the middle of the ablation over time. A total of n = 14 ablation sites from 14 spinal cords were analyzed and expressed as mean ± standard error of the mean (SEM). Bystander loss of axons (distance between the closest intact axons on both sides of the ablation site) minus the ablation site width (that remains constant over the 4-hour assessment time) was measured from a total of n = 3 to 14 ablation sites from 3 to 14 animals per group, analyzed, and expressed as mean ± SEM. The data from Figure 1J were used for the comparisons to treatment in Figure 4. Ca^{2+} measurements (X-rhod-1 AM) were taken along the length of YFP^+ axons over time beginning from the end bulb. Observed Ca^{2+} intensities (F) over time and distance from the end bulb were normalized to baseline (F_0) axonal recordings and reported as mean F/F_0; n = 21 to 22 axons undergoing pan-fragmentation or dieback,

respectively, were assessed. All experimenters who analyzed images in this study were blind to treatment.

Immunofluorescence

Slides of cryosectioned, fixed spinal cord sections underwent antigen retrieval utilizing sodium citrate, were blocked in 5% bovine serum albumin, and were incubated with rabbit anti-GRP78 BiP primary antibody (catalog number ab21685; Abcam, Cambridge, MA) at a final concentration of 1μg/ml in phosphate-buffered saline overnight at 4°C. Slides were washed and incubated with secondary antibody (1:1,000, Alexa Fluor 660 Goat Anti-Rabbit IgG; Life Technologies) for 2 hours at room temperature and mounted in Prolong Gold with 4′,6-diamidino-2-phenylindole.

Statistics

Axonal dieback data were analyzed with a Kruskal–Wallis 1-way analysis of variance (ANOVA) on ranks with Dunn's method of multiple comparisons versus aCSF control group, as the data failed normality. Width of axonal loss was compared between groups using an ANOVA, with a Holm–Sidak multiple comparison test versus aCSF control. Ablation area, ablation width, and width of axonal loss from aCSF-treated spinal cords were compared over time using a *t* test. Quantification of intra-axonal Ca^{2+} measurements was compared with a Mann–Whitney rank sum test. Probability values < 0.05 were considered significant.

Results

LiSCI Promotes Axonal Dieback and Secondary Axonal Degeneration

To reliably quantify axoglial damage over space and time, we devised a 2-photon Li-SCI model using live ex vivo murine spinal cords from transgenic mice that express YFP in dorsal column axons. An area on the dorsal surface of the cord measuring $\sim 18 \times 18\,\mu$m was irradiated, creating a well-defined and reproducible lesion (see Fig 1 and Supplementary Fig 1). Myelin was visualized by staining with Nile Red, and Ca^{2+} changes were measured using the cell-permeable Ca^{2+} indicator X-rhod-1 AM (K_d ~700 nM) or the membrane impermeable dextran-conjugated Oregon Green 488 BAPTA-1 (K_d ~170 nM; both from Life Technologies, Grand Island, NY) to detect robust and smaller discrete Ca^{2+} changes near axonal resting levels (~100 nM), respectively. This allowed us to observe and quantify immediate and delayed damage to central myelinated fibers over time with high spatial resolution. In control conditions, time-lapse recordings of the dorsal surface of the living spinal cord revealed parallel axons ensheathed in myelin, with few spheroids or other morphological signs of axonal degeneration for up to 7 hours. LiSCI induced immediate direct axonal transection at the irradiation site, then a delayed and progressive axonal dieback of transected axons proximal and distal to injury (Supplementary Video). In addition, indirect bystander degeneration of axons adjacent to the ablation site was observed, which increased over time. For clarity, all images in all figures are orientated so the proximal (caudal) segment of the axons that die back are in the top part of the panel, whereas the distal (rostral) axonal segments are at the bottom; the latter eventually undergo Wallerian degeneration at 24 to 48 hours after injury.

Importantly, the area of the primary ablation site remained static, whereas axonal damage and loss significantly increased over time, allowing the distinction between primary and secondary injury (see Fig 1J). Utilizing spectral confocal microscopy, the ablation site exhibited the spectral signatures of both lipofuscin and Nile Red (data not shown), presumably from degenerated cellular components and myelin, respectively, thus appearing bright red in the images. Thus, LiSCI is a highly reproducible model offering great spatiotemporal precision to examine mechanisms of direct and indirect axomyelinic injury in real time, immediately postinsult, which is impossible to do with most other conventional SCI models (see Fig 1 and Supplementary Fig 1).

We next examined the spatial and temporal dynamics of axonal dieback proximal and distal to the injury site. As reported previously using a mechanical injury model,[3] we observed that a proportion (~30%) of axons underwent a rapid pan-fragmentazation, that is, a synchronized beading and dissolution rather than a gradual dieback, both proximal and distal to the injury beginning 20 to 30 minutes after ablation (Fig 2A). In contrast, the majority (~70%) of transected axons instead underwent a gradual dieback of their axonal shaft within a ballooned myelin sheath (see Fig 2A–C); the axonal dieback extended up to 100 μm from the injury site after 4 hours. An illustration of the different patterns of axonal injury is shown in Figure 1K.

Calcium Dynamics in Injured Axons following LiSCI

Both activation of proteases (eg, calpains)[3] and microtubule instability[2] have been implicated in axonal dieback following SCI. Because intra-axonal Ca^{2+} rises may activate calpain and destabilize microtubules, we examined axonal Ca^{2+} dynamics following LiSCI by measuring Ca^{2+} changes in end bulbs and the proximal axonal shaft using fluorescent Ca^{2+} indicators. As shown in Figure 2, a pronounced increase in fluorescence was observed as early as 2 minutes following LiSCI in end bulbs and along the proximal axonal shaft remote from the ablation site within axons undergoing gradual dieback. Peak Ca^{2+}

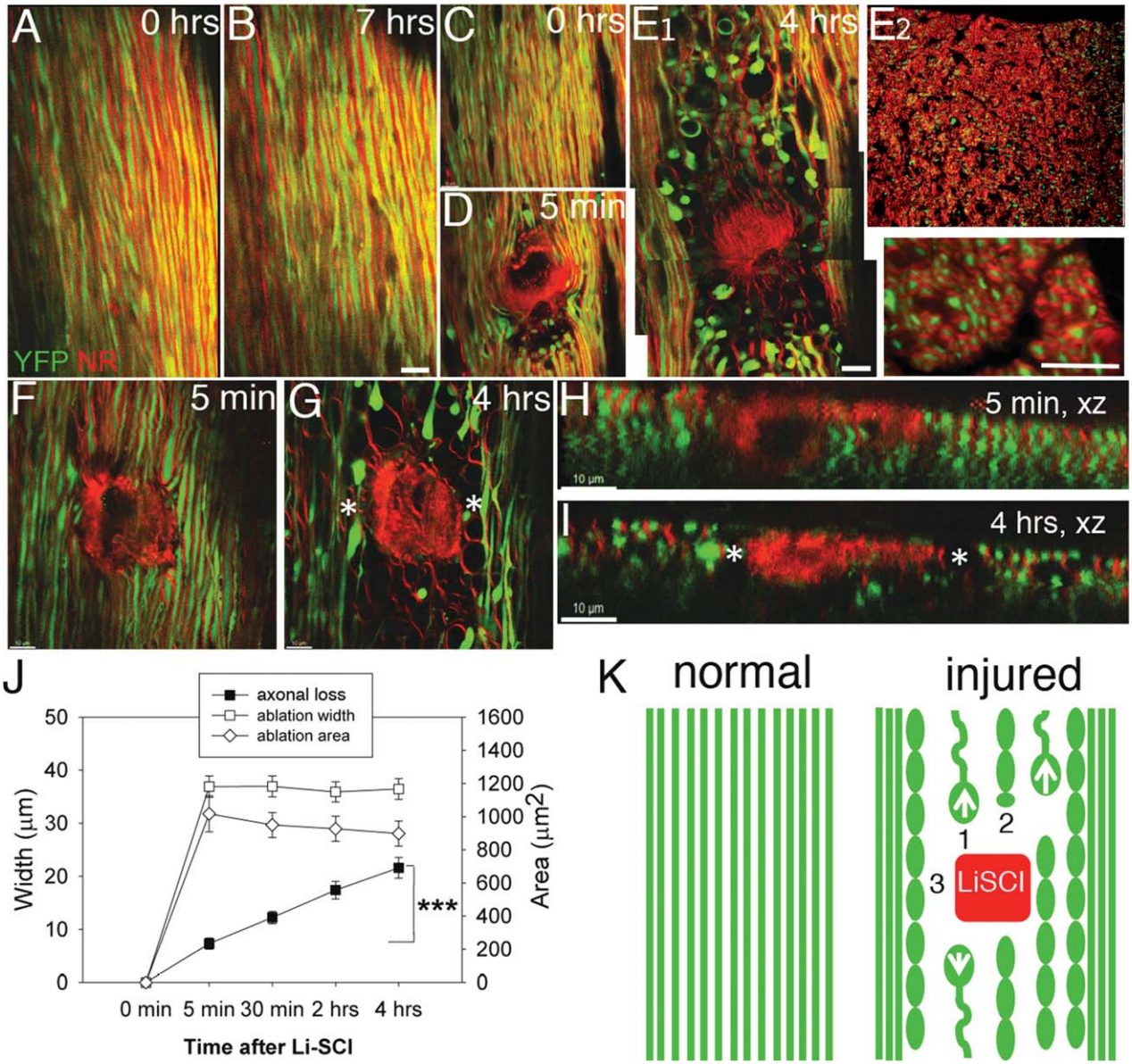

FIGURE 1: Laser-induced spinal cord injury (LiSCI) induces dieback and secondary degeneration of axons. (A, B) Live imaging of spinal cord under control conditions revealed parallel-aligned dorsal column axons (green, yellow fluorescent protein [YFP]$^+$) ensheathed in myelin (red, Nile Red [NR]). (C–I) LiSCI causes axonal dieback (C–E1) and secondary bystander damage of axons *(asterisks)* adjacent to the ablation site (F–I). (E2) Transverse section of the dorsal column (top) and high magnification of myelinated axons (bottom) reveals that Nile Red labels myelin that immediately ensheathes axons. The x–z plane is shown in H and I for F and G, respectively. (J) The site of primary injury (ablation width and area) does not change over time, allowing the distinction between primary and secondary injury (damage to adjacent fibers) in real time. Mean ± standard error of the mean, *t* test, ***$p < 0.001$, n = 14. (K) Illustration describing changes in transected axons that gradually die back (1) or synchronously fragment (2) over time. Adjacent to the ablation site, fibers that were originally uninjured may undergo delayed secondary degeneration (3). Scale bars = 10μm.

levels occurred within the end bulbs and tapered off as a function of distance from the end bulb, approaching baseline levels recorded preinjury. Conversely, robust Ca^{2+} elevations were seen within fibers undergoing pan-fragmentation, synchronously along the entire length of the degenerating fiber many tens of microns from the injury site. Furthermore, Ca^{2+} rises along the length of the axons, within the field of view, undergoing pan-fragmentation ($F/F_0 = 3.86 \pm 0.35$, mean ± SEM; n = 22 axons) remote from injury (>30 μm), were significantly ($p < 0.001$, Mann–Whitney rank sum test) higher than axons undergoing slow dieback ($F/F_0 = 1.37 \pm 0.10$; n = 21 axons) at 1 hour after LiSCI.

To further substantiate these findings, we bath-loaded axon cylinders in dorsal column or whole spinal cords with the membrane-impermeable Ca^{2+} indicator

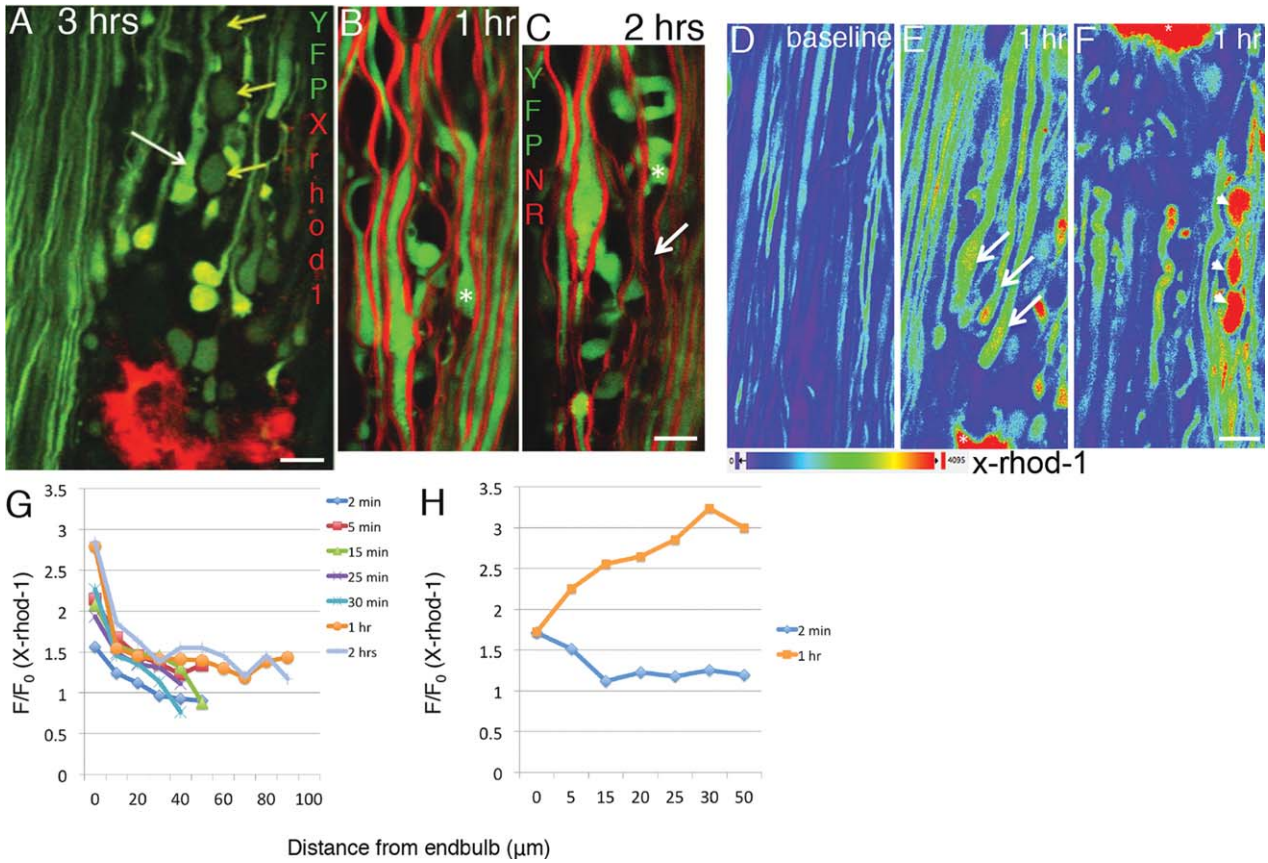

FIGURE 2: Pan-fragmentation and slow dieback of axons after laser-induced spinal cord injury (LiSCI). (A) Transected axons (yellow fluorescent protein [YFP]$^+$) underwent pan-fragmentation (~30%, *yellow arrows*) or slow dieback (~70%, *white arrow*). (B, C) Injured YFP$^+$ axons become separated from the myelin sheath (red) and retract the end bulb *(asterisks)* over time, leaving an empty myelin tube (*arrow,* same axon as in B). LiSCI-induced Ca^{2+} (X-rhod-1) increases over time are located within end bulbs and the proximal shaft in axons undergoing dieback (*arrows* in E; mean F/F_0, n = 22 [G]). (D) Baseline Ca^{2+} measurements. Pan-fragmenting axons experience increased Ca^{2+} along the length of the axon (*arrowheads* in F). Plot from a representative pan-fragmenting axon is shown in H over time. Note that D–F are representative images from different spinal cords than shown in A–C. Ca^{2+} signal (X-rhod1) channel is shown using a rainbow lookup table to reflect increasing intensity from 0 (violet) to 4095 (red). NR = Nile Red. Scale bars = 10μm. See also Supplementary Figures 2 and 3.

Oregon Green 488 BAPTA-1 dextran (10,000 MW) and an axonal tracer, dextran-conjugated Alexa 594 (10,000 MW) to follow dynamic Ca^{2+} events within the axoplasm of damaged axons.[8,13–15] In agreement with the X-rhod-1 results, time-lapse recordings showed pronounced increases of axonal Ca^{2+}-dependent fluorescence (~40%) acutely after injury in axonal end bulbs and shafts undergoing dieback (Supplementary Fig 2). Most axons undergoing pan-fragmentation showed increased Ca^{2+} signals within swollen axonal spheroids (Supplementary Fig 3). Together, these results indicate that axons undergoing gradual dieback exhibit a robust Ca^{2+} increase within the proximal end bulbs, with a steep Ca^{2+} gradient extending from the injury site (see Fig 2G). In distinction, fibers undergoing pan-fragmentation, whether directly transected or surviving the initial ablation but then succumbing to secondary bystander degeneration, experience robust Ca^{2+} changes along the length of the fiber.

Ryanodine and IP_3 Receptors Promote Axonal Dieback

We next examined the source of Ca^{2+} that led to intra-axonal Ca^{2+} accumulation and subsequent axonal degeneration. Ca^{2+} accumulation in axons may occur from the extracellular space by permeation across the axolemma, and from internal Ca^{2+} stores.[16,17] To test the effects of external Ca^{2+}, we altered Ca^{2+} concentration in the perfusate. Surprisingly, neither low (0.1 mM) nor zero Ca^{2+} aCSF (+0.5 mM ethyleneglycoltetraacetic acid) prevented axonal dieback at 4 hours after injury, although the former was protective at 1 hour (Fig 3). This finding suggests that either Ca^{2+} does not play an important role in axonal dieback, or that internal Ca^{2+} stores may contribute. Potential sources of intra-axonal Ca^{2+} release include the endoplasmic reticulum (ER) and mitochondria (reviewed in Stirling and Stys[17]). Both RyRs and inositol trisphosphate (IP_3) receptors mediate Ca^{2+} release from the

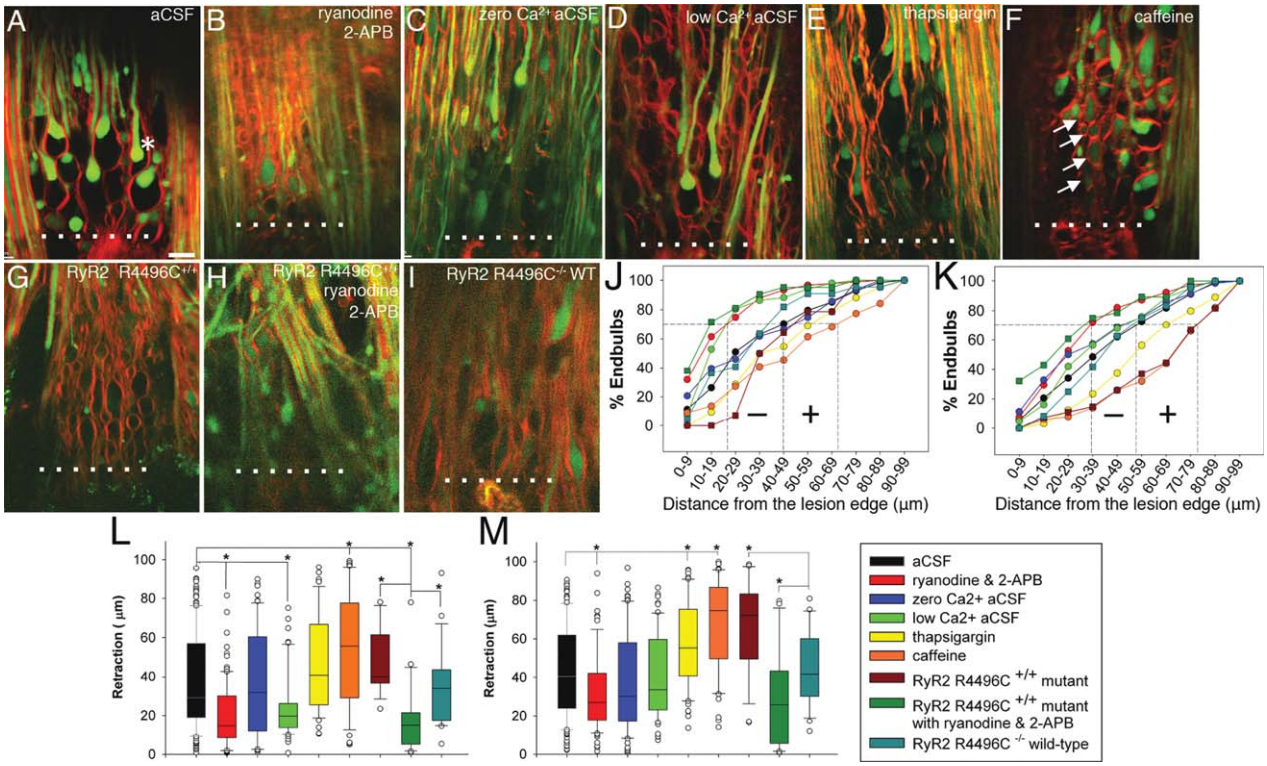

FIGURE 3: Axonal Ca^{2+} stores induce axonal dieback. (A–I) Representative images of live spinal axons (yellow fluorescent protein positive [A–F]; Alexa 488 conjugated dextran [G–I]) ensheathed in myelin (Nile Red) at 4 hours following laser-induced spinal cord injury (LiSCI). Only end bulbs connected to their proximal shaft *(asterisk)* and not isolated segments (arrows in F) were used to assess dieback distance from the edge of lesion *(ellipses)*. Scale bar = 10μm. (J, K) Cumulative distribution graphs of proximal axonal dieback at 1 (J) and 4 hours (K) following LiSCI. Inhibiting axonal Ca^{2+} stores (ryanodine and 2-aminoethoxydiphenylborane [2-APB]) shifts the distribution to the left (ie, less axonal dieback, −), whereas promoting intra-axonal Ca^{2+} release shifts the distribution to the right (ie, more axonal dieback, +) compared to artificial cerebrospinal fluid (aCSF) controls. (L, M) Ryanodine (50μM) and 2-APB (100μM) significantly reduced dieback at 1 (L) and 4 hours (M) following LiSCI. Neither low Ca^{2+} aCSF nor zero Ca^{2+} aCSF (0.5mM ethyleneglycoltetraacetic acid) reduced dieback at 4 hours. In distinction, treatments that prevented reuptake of intra-axonal Ca^{2+} (thapsigargin, 1μM) or promoted opening of ryanodine receptors (RyRs; caffeine, 0.5mM, RyR2 R4496C$^{+/+}$ knockin mice) significantly exacerbated axonal dieback at 1 and 4 hours. RyR2 R4496C$^{+/+}$ knockin mice treated with ryanodine and 2-APB reduced axonal dieback versus wild-type (WT) controls (M). Data are expressed as median and 25th and 75th percentile; Kruskal–Wallis 1-way analysis of variance on Ranks ($p < 0.001$), with Dunn's method of multiple comparisons versus control group (*$p < 0.05$), n = 24–141 axonal end bulbs per group.

ER,[18,19] and intra-axonal Ca^{2+} stores source Ca^{2+} in ischemic axons[8]; however, their contribution in SCI remains unknown. Blocking ryanodine and IP_3 receptors (ryanodine 50 μM + 2-APB 100 μM, respectively) beginning 30 minutes prior to LiSCI significantly reduced axonal dieback, implicating axonal Ca^{2+} stores over extracellular Ca^{2+} influx. Conversely, promoting Ca^{2+} release from stores either by blocking reuptake (thapsigargin 1 μM) or by opening RyRs (caffeine 0.5 mM) significantly worsened axonal dieback at 4 hours following LiSCI. We next examined whether a gain-of-function mutation in RyR2 (R4496C$^{+/+}$), which lowers the threshold for Ca^{2+} release from the RyR2 channel,[20] would alter axonal injury after LiSCI. We therefore utilized this gain-of-function knockin mouse line to assess the impact of spontaneous Ca^{2+} release mediated by the RyR2 R4496C$^{+/+}$ mutant on axonal injury following LiSCI. Spinal cords from homozygous R4496C$^{+/+}$ mice exhibited significantly more axonal dieback, to the high levels observed with caffeine at 4 hours. Notably, pretreatment of RyR2 R4496C$^{+/+}$ spinal cords with ryanodine and 2-APB to block Ca^{2+} release reduced dieback to levels comparable to wild-type cords treated with the same blockers. Together, these data support a central role of stored Ca^{2+} release in delayed axonal dieback following focal injury.

Ryanodine and IP_3 Receptors Promote Secondary Axonal Degeneration

To assess the role of intra-axonal Ca^{2+} store release in secondary bystander axonal degeneration,[21] we measured changes in lesion width and thus axonal loss adjacent to the ablation site as the lesion evolved over time. Importantly, our LiSCI model allowed the distinction between the direct primary injury that remained constant over time (see Fig 1) versus delayed damage of initially spared fibers. Unexpectedly, fibers adjacent to the primary lesion

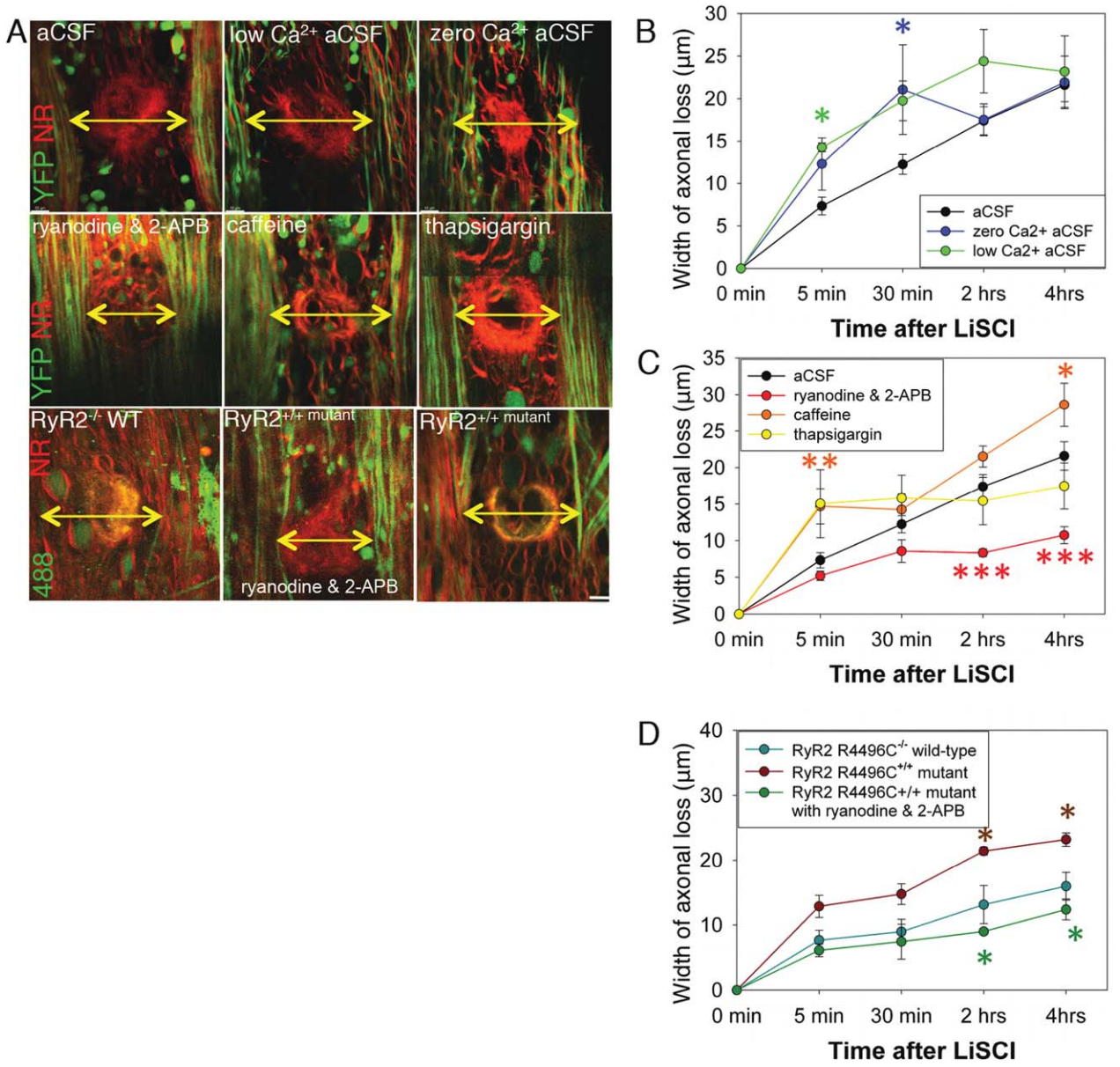

FIGURE 4: Axonal Ca^{2+} stores promote bystander damage. (A) Representative images of each treatment group at 4 hours post laser-induced spinal cord injury (LiSCI). The total lesion width *(yellow arrows)* is shown. The width of bystander axonal loss equals the total lesion width minus the ablation width. Scale bar = 10 μm. (B) Low or zero Ca^{2+} artificial cerebrospinal fluid (aCSF) potentiates axonal loss acutely. (C) Ryanodine and 2-aminoethoxydiphenylborane (2-APB) significantly reduced bystander damage at 2 and 4 hours after LiSCI. Caffeine worsened this effect. (D) Ryanodine receptor 2 (RyR2) R4496C$^{+/+}$ mutants experienced pronounced bystander damage compared to wild-type (WT) control mice and were rescued with ryanodine and 2-APB. Data are represented as mean ± standard error of the mean, analysis of variance (ANOVA), Holm–Sidak multiple comparisons versus aCSF control, *$p < 0.05$, **$p < 0.01$, ***$p < 0.001$; n = 3–14/group for B and C. RyR2 R4496C$^{+/+}$ mutant versus wild-type control or RyR2 R4496C$^{+/+}$ mutant treated with ryanodine and 2-APB, ANOVA, Holm–Sidak multiple comparisons, *$p < 0.05$; n = 2–5 per group in D. NR = Nile Red; YFP = yellow fluorescent protein.

site experienced increases in axonal Ca^{2+} levels similar to directly injured axons undergoing dieback (see Supplementary Fig 3). Of particular interest, both low Ca^{2+} and zero Ca^{2+} aCSF did not prevent secondary bystander loss of adjacent axons following LiSCI at 4 hours after injury, and instead exacerbated damage at earlier time points (see Fig 4). In line with mechanisms of axonal dieback described above, blocking intra-axonal store Ca^{2+} release (ryanodine + 2-APB) also significantly ($p < 0.001$) reduced bystander damage. Conversely, promoting Ca^{2+} release (caffeine) increased bystander axonal damage. Finally, as expected from the pharmacological experiments, R4496C$^{+/+}$ RyR2 gain-of-function mutants exhibited more bystander damage compared to wild-type

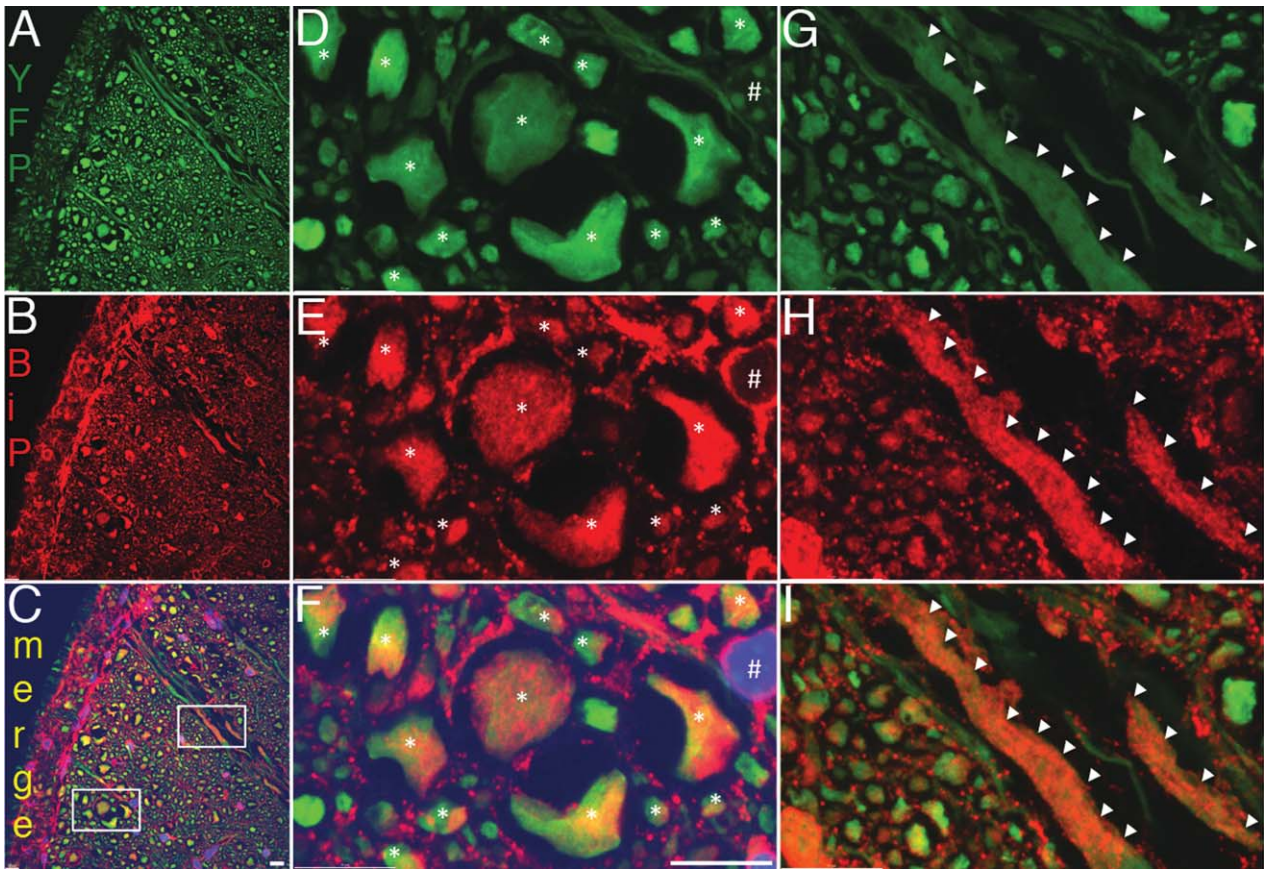

FIGURE 5: The endoplasmic reticulum (ER) chaperone protein BiP/GRP78 reveals the continuous nature of the endomembrane system within spinal axons. (A-C) Low magnification and (D-I) high magnification confocal images of transverse sections of spinal cord white matter from Thy1-YFP mice reveal that many axons (yellow fluorescent protein [YFP]$^+$, green) colocalize with the ER chaperone protein BiP/GRP78 (red) along the length of the axon. (D–F) Higher magnification of lower boxed region in C. Axons *(asterisks)* clearly contain BiP immunoreactivity as well as surrounding cells, presumably glia *(hash symbols)*. 4′,6-Diamidino-2-phenylindole (blue) is shown in panels C and F to reveal the nucleus of glial cells. (G–I) Higher magnification of upper boxed region in C reveals longitudinal axons originating from the dorsal root immunolabeled with BiP/GRP78 (red, *arrowheads*) along the length of the axon. Scale bars = 10μm.

controls, further supporting a key role of RyRs in several modes of delayed axonal injury. Intriguingly, these data suggest that both axonal dieback and secondary bystander degeneration of initially spared axons share common mechanisms heavily dependent on deregulation of axonal Ca^{2+} stores.

ER Marker BiP/GRP78 Is Localized within Spinal Cord Axons

Given that a significant proportion of fibers underwent a synchronous pan-degeneration beginning 20 to 30 minutes following LiSCI, this suggested that a deleterious injury signal may have been propagated from the focal ablation site to areas of damaged axons considerably removed from the site of injury. An extensive endomembrane system is present in axons consisting of a continuous network of ER that extends from the cell body to axonal terminals.[9,10,22] As shown in Figure 5, the ER marker BiP/GRP78[23] was localized to the axoplasm of many axons along the length of the fiber, providing support for the notion of an intra-axonal network that may propagate internal injury signals along injured axons.

Discussion

Taken together, our results implicate Ca^{2+} release from axonal Ca^{2+} stores as a key step in multiple delayed degenerative phenomena following focal axonal injury, heavily contributing to gradual dieback, synchronous delayed pan-degeneration, and bystander damage to initially uninjured fibers. Our primary focus was on the proximal (caudal) axons, as preventing dieback may have more relevance for regenerative mechanisms (growth cone formation and axonal regeneration), whereas the distal (rostral) segments will be destined for Wallerian degeneration. However, as shown in Figure 1E, axons proximal to the lesion (top) and distal (bottom) undergo similar dieback at these acute time points.

As the axonal pathology progresses over time, axonal Ca^{2+} stores can be continuously stimulated to release Ca^{2+} by a number of mediators known to be present in injured cord. The internodal axolemma of myelinated fibers expresses multimolecular nanocomplexes containing many signaling proteins, including glutamate receptors, nitric oxide synthase, RyRs, IP_3 receptors, and voltage-gated Ca^{2+} channels[14,15] (for review see Stirling and Stys[17]). It is well established that glutamate and nitric oxide accumulate in injured cord,[24,25] released from damaged axons[14,26] and from reactive microglia and immune cells recruited to the damaged area.[27,28] In addition, depolarization of injured axons will be sensed by internodal Ca^{2+} channels, further activating intra-axonal RyRs.[8] Other potential causes of bystander axonal damage cannot be excluded and may result from directly injured cells adversely influencing their neighboring axons. Examples of these may include a resultant increase in extracellular K^+ from adjacent directly injured cells that influence nearby axons or from the oligodendrocytes themselves that may ensheathe directly injured and bystander axons and transfer injury to the latter.

We found the *ex vivo* whole spinal cord model here advantageous, as it can be removed quickly without the additional steps needed to isolate the dorsal columns, prevents damage of the superficial dorsal column fibers that unavoidably occurs during dorsal column strip preparation, and allows for manipulation of the external ionic and pharmacological milieus necessary to assess the role of external Ca^{2+} sources versus intra-axonal Ca^{2+} stores. In support of the viability of the preparation, the morphology of the axons in our *ex vivo* preparation (see Fig 1) were identical to those of intact axons of the dorsal columns in vivo.[29] In addition, the white matter axons under study responded to LiSCI with calcium changes and morphological changes (spheroid formation and axonal dieback), all known active axonal responses to injury similar to what has been previously described in an SCI injury *in vivo* (See Erturk et al[29]; Fig 1F, G). Furthermore, only injured axons showed increased intra-axonal Ca^{2+} levels and not axons remote to the lesion site (see Fig 2 and Supplementary Fig 2). Although we cannot rule out that deeper locations of the whole cord may have gradually degenerated because of limited penetration of bath-supplied nutrients, others have shown that *ex vivo* spinal cord models are viable up to 3 weeks in culture.[30] Both whole brain and spinal cord models, from rodent and higher mammals such as dogs, have been used in electrophysiology experiments with demonstrated robust viability of these preparations for up to 8 hours after removal.[31]

The extensive network of the axoplasmic reticulum (see Fig 5)[9,22] may further propagate damage over distances considerably removed from the primary injury site. Finally, removal of external Ca^{2+}, a maneuver that is highly protective in other white matter injury paradigms,[32–35] was totally ineffective at reducing LiSCI pathology. This refocuses our approach to protecting spinal white matter tracts and emphasizes that for more focal injuries like SCI, modulation of axonal Ca^{2+} stores may be the more important pharmacotherapeutic target. This in turn may provide a strategy to prevent axonal dieback as a necessary step prior to promoting growth cone formation and axonal regeneration; given the reduction of the spatial extent of injury when internal Ca^{2+} release is restrained, both to directly damaged and bystander fibers, this may also assist in regenerative efforts, either spontaneous or experimentally induced. Lastly, targeting intra-axonal store Ca^{2+} release may also be applicable to other neurological diseases in which diffuse axonal injury or degenerative axonal loss contributes to morbidity.

Acknowledgment

Supported by a grant from the Leblanc Chair for Spinal Cord Injury. D.P.S. was supported by a grant from the Paralyzed Veterans of America Research Foundation. S.R.W.C. is an Alberta Innovates-Health Solutions Scientist, supported in part by research grants from the Canadian Institutes of Health Research. P.S. is the Leblanc Chair in Spinal Cord Research, Canada Research Chairs, Alberta Innovates-Health Solutions.

Authorship

D.P.S. conceptualized the live ex vivo spinal cord injury model, and D.P.S. and P.S. designed the experiments. D.P.S. carried out the live tissue imaging and performed the image analysis. K.C. performed the immunohistochemistry and image analysis. S.R.W.C. created the $R4496C^{+/+}$ knock-in mice. D.P.S., P.S., and S.R.W.C. cowrote the manuscript.

Potential Conflicts of Interest

Nothing to report.

References

1. Waller A. Experiments on the section of the glossopharyngeal and hypoglosal nerves of the frog, and observations of the alterations produced thereby in the structure of their primitive fibres. Philos Trans R Soc Lond 1850;140:423–429.

2. Hellal F, Hurtado A, Ruschel J, et al. Microtubule stabilization reduces scarring and causes axon regeneration after spinal cord injury. Science 2011;331:928–931.

3. Kerschensteiner M, Schwab ME, Lichtman JW, Misgeld T. In vivo imaging of axonal degeneration and regeneration in the injured spinal cord. Nat Med 2005;11:572–577.
4. Busch SA, Horn KP, Silver DJ, Silver J. Overcoming macrophage-mediated axonal dieback following CNS injury. J Neurosci 2009; 29:9967–9976.
5. Stirling DP, Khodarahmi K, Liu J, et al. Minocycline treatment reduces delayed oligodendrocyte death, attenuates axonal dieback, and improves functional outcome after spinal cord injury. J Neurosci 2004;24:2182–2190.
6. McPhail LT, Stirling DP, Tetzlaff W, et al. The contribution of activated phagocytes and myelin degeneration to axonal retraction/dieback following spinal cord injury. Eur J Neurosci 2004;20:1984–1994.
7. Verma P, Fawcett J. Spinal cord regeneration. Adv Biochem Eng Biotechnol 2005;94:43–66.
8. Ouardouz M, Nikolaeva MA, Coderre E, et al. Depolarization-induced Ca2+ release in ischemic spinal cord white matter involves L-type Ca2+ channel activation of ryanodine receptors. Neuron 2003;40:53–63.
9. Terasaki M, Slater NT, Fein A, et al. Continuous network of endoplasmic reticulum in cerebellar Purkinje neurons. Proc Natl Acad Sci U S A 1994;91:7510–7514.
10. Broadwell RD, Cataldo AM. The neuronal endoplasmic reticulum: its cytochemistry and contribution to the endomembrane system. II. Axons and terminals. J Comp Neurol 1984;230:231–248.
11. Boulnois JL. Photophysical processes in recent medical laser developments: a review. Laser Med Sci 1986;1:47–66.
12. Loesel FH, Fischer JP, Gotz MH, et al. Non-thermal ablation of neural tissue with femtosecond laser pulses. Appl Phys B 1998;66: 121–128.
13. Ren Y, Ridsdale A, Coderre E, Stys PK. Calcium imaging in live rat optic nerve myelinated axons in vitro using confocal laser microscopy. J Neurosci Methods 2000;102:165–176.
14. Ouardouz M, Coderre E, Zamponi GW, et al. Glutamate receptors on myelinated spinal cord axons: II. AMPA and GluR5 receptors. Ann Neurol 2009;65:160–166.
15. Ouardouz M, Coderre E, Basak A, et al. Glutamate receptors on myelinated spinal cord axons: I. GluR6 kainate receptors. Ann Neurol 2009;65:151–159.
16. Tsutsui S, Stys PK. Metabolic injury to axons and myelin. Exp Neurol 2013;246:26–34.
17. Stirling DP, Stys PK. Mechanisms of axonal injury: internodal nanocomplexes and calcium deregulation. Trends Mol Med 2010;16: 160–170.
18. Berridge MJ. Inositol trisphosphate and calcium signalling. Nature 1993;361:315–325.
19. Cheng H, Lederer WJ, Cannell MB. Calcium sparks: elementary events underlying excitation-contraction coupling in heart muscle. Science 1993;262:740–744.
20. Jiang D, Xiao B, Yang D, et al. RyR2 mutations linked to ventricular tachycardia and sudden death reduce the threshold for store-overload-induced Ca2+ release (SOICR). Proc Natl Acad Sci U S A 2004;101:13062–13067.
21. Profyris C, Cheema SS, Zang D, et al. Degenerative and regenerative mechanisms governing spinal cord injury. Neurobiol Dis 2004; 15:415–436.
22. Ramirez OA, Couve A. The endoplasmic reticulum and protein trafficking in dendrites and axons. Trends Cell Biol 2011;21: 219–227.
23. Villa A, Podini P, Clegg DO, et al. Intracellular Ca2+ stores in chicken Purkinje neurons: differential distribution of the low affinity-high capacity Ca2+ binding protein, calsequestrin, of Ca2+ ATPase and of the ER lumenal protein, Bip. J Cell Biol 1991;113:779–791.
24. Hamada Y, Ikata T, Katoh S, et al. Roles of nitric oxide in compression injury of rat spinal cord. Free Radic Biol Med 1996;20:1–9.
25. Xu GY, Hughes MG, Ye Z, et al. Concentrations of glutamate released following spinal cord injury kill oligodendrocytes in the spinal cord. Exp Neurol 2004;187:329–336.
26. Li S, Mealing GA, Morley P, Stys PK. Novel injury mechanism in anoxia and trauma of spinal cord white matter: glutamate release via reverse Na+-dependent glutamate transport. J Neurosci 1999; 19:RC16.
27. Hermann GE, Rogers RC, Bresnahan JC, Beattie MS. Tumor necrosis factor-alpha induces cFOS and strongly potentiates glutamate-mediated cell death in the rat spinal cord. Neurobiol Dis 2001;8:590–599.
28. Satake K, Matsuyama Y, Kamiya M, et al. Nitric oxide via macrophage iNOS induces apoptosis following traumatic spinal cord injury. Brain Res Mol Brain Res 2000;85:114–122.
29. Erturk A, Hellal F, Enes J, Bradke F. Disorganized microtubules underlie the formation of retraction bulbs and the failure of axonal regeneration. J Neurosci 2007;27:9169–9180.
30. Krassioukov AV, Ackery A, Schwartz G, et al. An in vitro model of neurotrauma in organotypic spinal cord cultures from adult mice. Brain Res Brain Res Protoc 2002;10:60–68.
31. Kerkut GA, Bagust J. The isolated mammalian spinal cord. Prog Neurobiol 1995;46:1–48.
32. Stys PK, Ransom BR, Waxman SG, Davis PK. Role of extracellular calcium in anoxic injury of mammalian central white matter. Proc Natl Acad Sci U S A 1990;87:4212–4216.
33. Waxman SG, Black JA, Ransom BR, Stys PK. Protection of the axonal cytoskeleton in anoxic optic nerve by decreased extracellular calcium. Brain Res 1993;614:137–145.
34. Imaizumi T, Kocsis JD, Waxman SG. Anoxic injury in the rat spinal cord: pharmacological evidence for multiple steps in Ca(2+)-dependent injury of the dorsal columns. J Neurotrauma 1997;14: 299–311.
35. Brown AM, Fern R, Jarvinen JP, et al. Changes in [Ca2+]0 during anoxia in CNS white matter. Neuroreport 1998;9:1997–2000.
36. Zhou Q, et al. Carvedilol and its new analogs suppress arrhythmogenic store overload-induced Ca^{2+} release. Nat Med 2011;17: 1003–1009.